Reflection Impedance

Lúcio T. Santos, Martin Tygel, IMECC/UNICAMP, and Antonio C. Buginga Ramos, PETROBRAS S/A, Brazil*

Abstract

AVO is now an established technology and has been widely deployed as a lithology indicator and also as a direct hydrocarbon indicator. In recent years this technology has become a routine processing and its application to large 3D volumes has relied on the use of near- and far-offset stack volumes. These volumes greatly reduce the amount of prestack information that needs to be stored for standard AVO processing. Additionally, these volumes are easily converted into usual AVO attributes, like intercept and gradient, which can then be interpreted in terms of anomalies and calibrated with well logs. Reservoir characterization studies make use not only of these traditional AVO attributes but also impedance volumes. The near-offset, or the intercept, stack volume offers a natural way of obtaining acoustic impedance volume through the use of post-stack inversion algorithms. However, to invert far-stack volume one needs an approach capable of estimating impedances for a variable incidence angle. This approach has been described in the elastic impedance function presented by Connolly (1999). In this work we propose an approach called reflection impedance, which is based on constant ray parameter and a power relationship between density and S-wave velocity. This new method proved to be of better accuracy for angular impedance estimation and reflection coefficient recovery when compared with the elastic impedance approach.

Introduction

In recent years there has been an enormous increase in the amount of 3D seismic data processed with AVO purpose. The most economical form of processing large volumes of seismic data to obtain AVO attributes involves obtaining near- and far-offset stacks. These stacks have been intensively used not only to obtain traditional AVO attributes, like intercept and gradient, but also as input of post-stack inversion algorithms to yield acoustic impedance (AI) volumes that help in reservoir characterization. The near-offset stack can be tied to synthetics obtained from acoustic impedance changes derived from well logs. After calibration, the near-offset stacks can then be inverted back to acoustic impedances using off-the-shelf post-stack inversion algorithms, which use the well log impedances as constraints. The missing part of this process was how to invert the far-offset stacks? The answer to the question came from the elastic impedance (EI) approach presented by Connolly (1999), which generalizes the acoustic impedance concept for variable incidence angle. In other words, the EI provides a way to calibrate and invert nonzero-offset seismic data just as AI does for zero-offset data. One advantage of the EI method is that it correlates directly to rock properties, like α/β ratio (P- to S-wave velocity ratio), instead of being an attribute that relates to contrasts of elastic properties of neighboring rocks (like most AVO attributes).

In this work we demonstrate a new approach to obtain nonzero-offset impedance estimates to be used as calibration for nonzero-offset seismic data. We called this approach reflection impedance (RI). Basically, RI is based on constant ray parameter as opposed to constant incidence angles, as proposed by Connolly (1999). Also, the new approach assumes a power relation between density and S-wave velocity while the EI approach assumes a constant $K=(\beta/\alpha)^2$. As a result, the new approach greatly improves the accuracy of the impedance estimates, which can be critical in case of subtle amplitude anomalies.

Normal Incidence: Acoustic and Elastic

For a given normal reflected ray, parameterized by the depth z, the normal P-P reflection coefficient is given by

$$R(z,\Delta z)=\frac{AI(z+\Delta z)-AI(z)}{AI(z+\Delta z)+AI(z)} \qquad (1)$$

where

$$AI(z)=\rho(z)\,\alpha(z) \qquad (2)$$

is the acoustic impedance function, $\rho(z)$ is the density function, $\alpha(z)$ is the P-wave velocity function, and Δz is the depth increment, chosen to be sufficiently small. Observe that we also consider that the elastic parameters are being parameterized by the depth.

Reflection Incidence: Acoustic

For a general incidence angle, $\theta(z)$, the acoustic reflection coefficient, $R_\theta(z, \Delta z)$ can be written in the same form as equation (1), namely,

$$R_\theta(z,\Delta z)=\frac{RI_\theta(z+\Delta z)-RI_\theta(z)}{RI_\theta(z+\Delta z)+RI_\theta(z)}, \qquad (3)$$

with the exception that the reflection impedance of angle θ, $RI_\theta(z)$, defined by

$$RI_\theta(z)=\rho(z)\,\alpha(z)\sec\theta(z), \qquad (4)$$

replaces the previous acoustic impedance, $AI(z)$. Observe that the reflection impedance reduces to the acoustic impedance in the case $\theta=0$, namely $RI_{\theta=0}=AI$. Introducing the ray parameter, $p = \sin\theta(z)/\alpha(z)$, the reflection impedance can be recast in the form

$$RI_p(z)=\frac{\rho(z)\alpha(z)}{\sqrt{1-\alpha^2(z)p^2}}. \qquad (5)$$

Reflection Impedance

Elastic Impedance

Connolly (1999) starts the derivation of the EI_θ (elastic impedance) function by approximating the P-P reflection coefficient given in Aki and Richards (1980) by

$$R_\theta(z,\Delta z) \approx \frac{EI_\theta(z+\Delta z) - EI_\theta(z)}{EI_\theta(z+\Delta z) + EI_\theta(z)} \approx \frac{1}{2}\,\Delta \ln(EI_\theta)\,. \qquad (6)$$

Replacing the exact reflection coefficient by its linearized approximation and assuming the conditions of constant angle, θ, and constant ratio, $K = \beta^2(z)/\alpha^2(z)$, of S- and P-velocities $\beta(z)$ and $\alpha(z)$, respectively, the solution of the above difference equation can be written

$$EI_\theta = \rho_0\alpha_0 \left(\frac{\rho}{\rho_0}\right)^{(1-4K\sin^2\theta)} \left(\frac{\alpha}{\alpha_0}\right)^{(\sec^2\theta)} \left(\frac{\beta}{\beta_0}\right)^{(-8K\sin^2\theta)}. \qquad (7)$$

Here, ρ_0, α_0 and β_0 are properly chosen density and velocity constants, respectively. See Mallick (2001) and Whitcombe (2002) for more details.

Reflection Impedance: Elastic

The concept of reflection impedance is in essence similar to the EI_θ function presented above. We consider the approximation

$$R_\theta(z,\Delta z) \approx \frac{RI_\theta(z+\Delta z) - RI_\theta(z)}{RI_\theta(z+\Delta z) + RI_\theta(z)} \qquad (8)$$

which implies that

$$\lim_{\Delta z \to 0} \frac{R_\theta(z,\Delta z)}{\Delta z} = \frac{1}{2}\frac{RI'_\theta(z)}{RI_\theta(z)}, \qquad (9)$$

where the prime denotes derivative with respect to z. Computing the left-hand side limit, using the exact reflection coefficient formula, yields a differential equation analogous to the difference equation (6). We solve the resulting equation under the assumptions of constant ray parameter, p, together with a dependency between density and S-wave velocity of the form $\rho(z) = b\,\beta(z)^\gamma$, with b and γ as empirical constants to be determined. We find

$$RI_\theta = \rho\,\alpha\,\sec\theta\,\exp\left[-2(2+\gamma)\left(\frac{\beta}{\alpha}\right)^2 \sin^2\theta\right], \qquad (10)$$

or, using the ray parameter, p, instead of the angle, θ,

$$RI_p = \frac{\rho\,\alpha}{\sqrt{1-\alpha^2 p^2}}\,\exp\left[-2(2+\gamma)\,\beta^2 p^2\right]. \qquad (11)$$

Note that in the acoustic case (in which $\beta=0$), the reflection impedances (10) –(11) reduces to their corresponding expressions (4)-(5).

Discussion

In order to compare the accuracy of EI_θ and RI_θ functions presented above we use the approximation of P-P elastic reflection at a point between two media with local parameters given by ρ_i, α_i, β_i, with i representing the layer index in each side of the interface, such that:

$$R_{PP}^{EI} \cong \frac{EI_2 - EI_1}{EI_2 + EI_1} \quad \text{and} \quad R_{PP}^{RI} \cong \frac{RI_2 - RI_1}{RI_2 + RI_1}. \qquad (12)$$

Here, to compute RI we used the following formula for γ:

$$\gamma = \ln(\rho_2/\rho_1) \,/\, \ln(\beta_2/\beta_1) \approx (\Delta\rho/\rho)/(\Delta\beta/\beta). \qquad (13)$$

The models used in the computations are shown in Table 1. They were chosen from a suite of 25 sets of models given in Castagna and Smith (1994), and represent three different AVO classes. The results are shown in Figures 1 to 3. The response computed based on the elastic impedance method deviates not only from the exact Zoeppritz formula for reflection coefficients but also from the linearized approximation (Shuey, 1985) for R_{pp}. The response computed from the reflection impedance method agrees with the exact Zoeppritz formula for R_{pp}. Therefore there is a significant gain in accuracy provided by the reflection impedance method compared to the elastic impedance method.

Class	Rock	α (km/s)	β (km/s)	ρ (g/cm^3)
I	Gas sand	4.05	2.38	2.32
	Brine sand	4.35	2.34	2.40
	Shale	2.77	1.52	2.30
II	Gas sand	2.69	1.59	2.25
	Brine sand	3.05	1.56	2.40
	Shale	2.77	1.27	2.45
III	Gas sand	1.44	0.58	1.53
	Brine sand	2.13	0.67	1.90
	Shale	1.83	0.40	2.02

Table 1 – Elastic properties used to model EI and RI curves

Figure 4 shows the well log data from an oil sand reservoir (dashed box) encased in marine shales. In Figure 5 we show the comparison of the AI curve with the normalized EI(30°) and RI(30°) curves. Normalization was done following Whitcombe (2002) in both cases. The normalized EI and RI curves are very similar outside the reservoir zone, but disagree in the reservoir zone, possibly because the RI method senses more the changes in β/α ratio. Therefore, the observed differences are in part related to the higher degree of accuracy obtained by the RI method compared to the EI method. The apparent improved discrimination of the reservoir zone in the RI curve can be a key for the use of this method instead of the EI.

Conclusions

The RI method proved that it recovers back the exact reflection coefficient curve from a simple form of approximation. Additionally, when used to produce angle dependent impedances, the proposed RI method showed greater accuracy

and improved degree of discrimination compared to the EI method.

References

Aki, K.I., and Richards, P. G.,1980, Quantitative Seismology, W.H. Freeman and Co.

Castagna, J. P., and Smith, S. W., 1994, Comparison of AVO Indicators: A Modeling Study, Geophysics, 59, 1849-1855.

Connolly, P., 1999, Elastic Impedance: The Leading Edge, v. 18, p. 448-452.

Mallick, S., 2001, AVO and Elastic Impedance, The Leading Edge, 20, 1094-1104.

Shuey, R. T., 1985, A Simplification of the Zoeppritz Equations, Geophysics, 50, 609-614.

Whitcombe, D. N., 2002, Elastic Impedance Normalization, Geophysics, 67, 60-62.

Acknowledgments

This work has been partially supported by FAPESP and CNPq (Brazil), the sponsors of the Wave Inversion Technology (WIT) Consortium. We thank PETROBRAS for permission to publish this work.

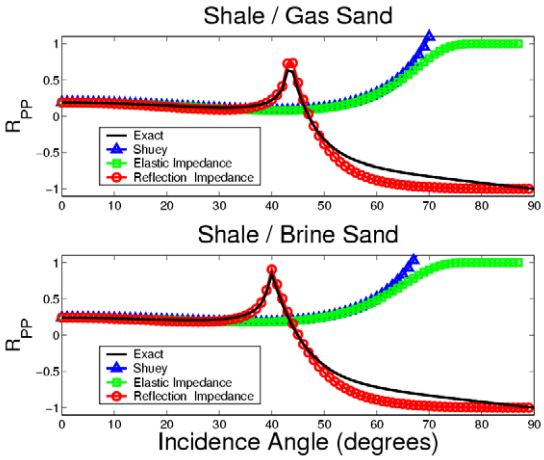

Figure 1- P-P reflection coefficient for Class I model given in Table 1: shale over gas sand (top) and shale over brine sand (bottom).

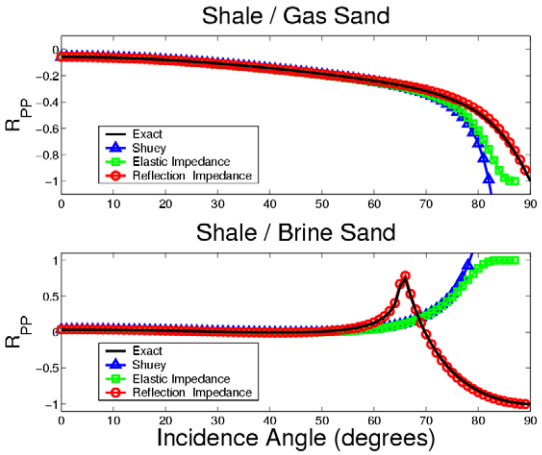

Figure 2- P-P reflection coefficient for Class II model given in Table 1: shale over gas sand (top) and shale over brine sand (bottom).

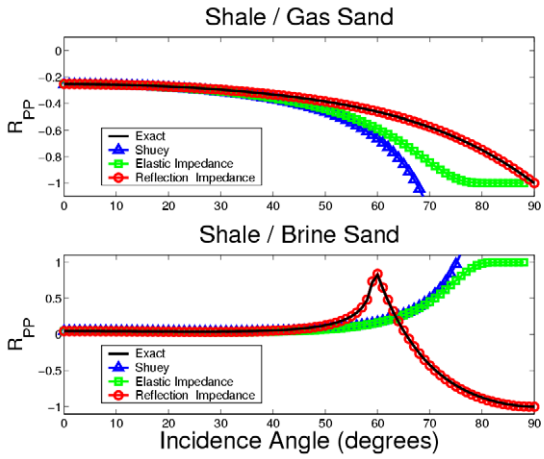

Figure 3- P-P reflection coefficient for Class III model given in Table 1: shale over gas sand (top) and shale over brine sand (bottom).

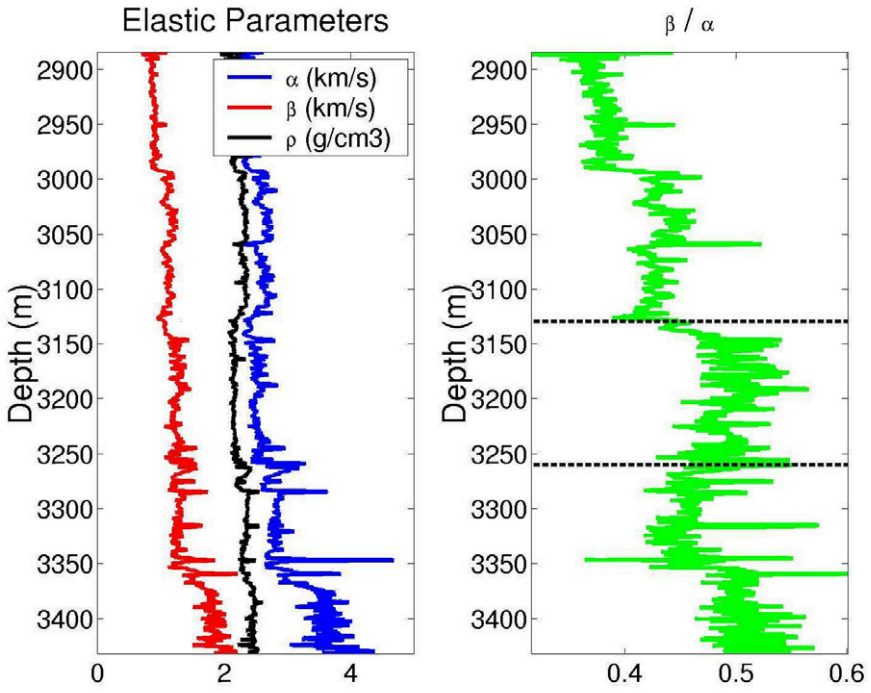

Figure 4 – Well log data of an oil sand reservoir (dashed box) encased in marine shales.

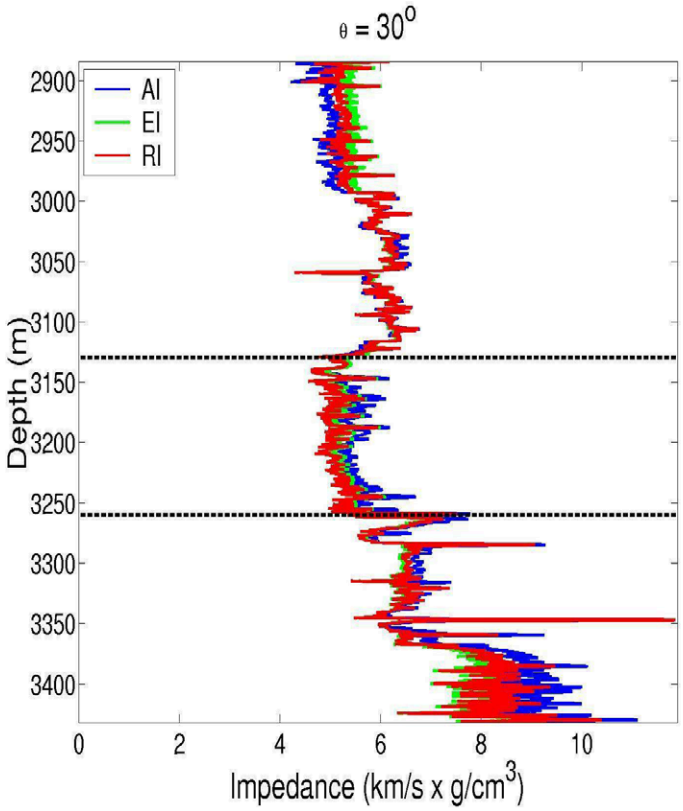

Figure 5 – Comparison of AI curve with normalized 30° EI and RI curves for the well log data given in Figure 4.